with hemodynamically relevant carotid artery stenosis (>70%). These effects, however, can be overlooked easily when using standard ROI analysis that is not individually tailored. This limitation becomes increasingly important as PET emerges as a clinical tool and clinicians search for easy methods to interpret PET studies for use in the clinical management of patients. In patients with carotid artery disease, physicians cannot afford to rely on computer-generated analysis programs alone but will also be required to visually assess studies on a case-by-case basis, since those patients who only demonstrate a visually detectable area of decreased perfusion and corresponding elevated oxygen and/or glucose extraction fraction ipsilateral to the carotid stenosis may still benefit from surgical intervention. Therefore, multiparametric PET assessment of the hemodynamic and metabolic status in patients with carotid stenosis should always include both careful visual and standard ROI analysis.

REFERENCES

1. Thompson JE, Patman RD, Talkington CM. Asymptomatic carotid bruit: long-term outcome of patients having endarterectomy compared with unoperated controls. *Ann Surg* 1978;188:308–316.
2. Humphries AW, Young JR, Santilli PH, Beven EG, de Wolfe VG. Unoperated, asymptomatic significant internal carotid stenosis: a review of 182 instances. *Surgery* 1976;80:695–698.
3. Chambers BR, Norris JW. Outcome in patients with asymptomatic neck bruits. *N Engl J Med* 1986;315:860–865.
4. Quinones-Baldrich WJ, Moore WS. Asymptomatic carotid stenosis: rationale for management. *Arch Neurol* 1985;42:378–382.
5. Gibbs JM, Wise RJS, Leenders KL, Jones T. Evaluation of cerebral perfusion reserve in patients with carotid artery occlusion. *Lancet* 1984;I:310–314.
6. Levine RL, Lagreze HL, Dobkin JA, et al. Cerebral vasocapacitance and TIAs. *Neurology* 1989;39:25–29.
7. Powers WJ, Press GW, Grubb RL Jr, Gado M, Raichle ME. The effect of hemodynamically significant carotid artery disease on the hemodynamic status of the cerebral circulation. *Ann Intern Med* 1987;106:27–35.
8. Powers WJ, Grubb RL Jr, Raichle ME. Clinical results of extracranial-intracranial bypass surgery in patients with hemodynamic cerebrovascular disease. *J Neurosurg* 1989;70:61–67.
9. Powers WJ, Tempel LW, Grubb RL. Influence of cerebral hemodynamics on stroke risk: one-year follow-up of 30 medically treated patients. *Ann Neurol* 1989;25:325–330.
10. Powers WJ. Cerebral hemodynamics in ischemic cerebrovascular disease. *Ann Neurol* 1991;29:231–240.
11. Carpenter DA, Grubb RL Jr, Powers WJ. Border zone hemodynamics in cerebrovascular disease. *Neurology* 1990;40:1587–1592.
12. Leblanc R, Yamamoto YL, Tyler JL, Diksic M, Hakim A. Borderzone ischemia. *Ann Neurol* 1987;22:707–713.
13. Leblanc R, Yamamoto YL, Tyler JL, Hakim A. Hemodynamic and metabolic effects of extracranial carotid disease. *Can J Neurol Sci* 1989;16:51–57.
14. Herholz K, Pietrzyk U, Wienhard K, et al. Regional cerebral blood flow measurement with intravenous ^{15}O-water bolus and ^{18}F-fluoromethane inhalation. *Stroke* 1989;20:1174–1181.
15. Herscovitch P, Markham J, Raichle ME: Brain blood flow measured with intravenous $H_2{}^{15}O$. I. Theory and error analysis. *J Nucl Med* 1983;24:782–729.
16. Mintun MA, Raichle ME, Martin WRW, Herscovitch P. Brain oxygen utilization measured with ^{15}O radiotracers and PET. *J Nucl Med* 1984;25:177–187.
17. Grubb RL, Raichle ME, Higgins CS, Eichling JO. Measurement of regional cerebral blood volume by emission tomography. *Ann Neurol* 1978;4:322–328.
18. Reivich M, Kuhl D, Wolf A, et al. The ^{18}F-fluorodeoxyglucose method for the measurement of local cerebral glucose utilization in man. *Circ Res* 1979;44:127–137.
19. Wienhard K, Pawlik G, Herholz K, Wagner R, Heiss W-D. Estimation of local cerebral utilization by positron emission tomography of ^{18}F-2-fluoro-2-deoxy-D-glucose: a critical appraisal of optimization procedures. *J Cereb Blood Flow Metab* 1985;5:115–125.
20. Heiss W-D, Pawlik G, Herholz K, Göldner H, Wienhard K. Regional kinetic constants and cerebral metabolic rate for glucose in normal human volunteers determined by dynamic PET of ^{18}F-2-fluoro-2-deoxy-D-glucose. *J Cereb Blood Flow Metab* 1984;4:212–223.
21. Heiss W-D, Huber M, Fink GR, et al. Progressive derangement of periinfarct viable tissue in ischemic stroke. *J Cereb Blood Flow Metab* 1992;12:193–203.
22. Pietrzyk U, Herholz K, Fink G, et al. Validation of a multi-purpose three-dimensional image registration program. *J Nucl Med* 1994;35:2011–2018.
23. Herholz K, Pawlik G, Wienhard K, Heiss WD. Computer assisted mapping in quantitative analysis of cerebral positron emission tomograms. *J Comput Assist Tomogr* 1985;9:154–161.
24. Damasio H. In: Wood J, ed. *Cerebral blood flow: physiologic and clinical aspects*. New York: McGraw-Hill; 1987:324–332.
25. Vander Eecken HM, Adams RD. Anatomy and functional significance of meningeal anastomoses of human brain. *J Neuropathol Exp Neurol* 1953;12:132–157.
26. Archie JP Jr, Feldtman RW. Critical stenosis of the internal carotid artery. *Surgery* 1981;89:67–70.
27. De Weese JA, May AG, Lipchik EO, Rob CG. Anatomic and hemodynamic correlations in carotid artery stenosis. *Stroke* 1970;1:149–157.
28. Boysen G, Ladegaard-Pedersen HJ, Valentin N, Engell HC. Cerebral blood flow and internal carotid artery flow during carotid surgery. *Stroke* 1970;1:253–260.
29. Huber M, Hojer C, Neveling M, Fink GR, Herholz K. Transcranial doppler and ^{15}O-water PET findings in patients with acute brain infarction and middle cerebral artery stenosis. *J Stroke Cerebrovasc Dis* 1994;4:23–29.
30. Friston KJ, Frith CD, Liddle PF, Frackowiak RSJ. Comparing functional PET images: the assessment of significant change. *J Cereb Blood Flow Metab* 1991;11:690–699.

Modeling of Fluorine-18-6-Fluoro-L-Dopa in Humans

Lindi Wahl and Claude Nahmias

Department of Nuclear Medicine, McMaster University Medical Centre Hamilton, Ontario, Canada

Fluorine-18-6-fluoro-L-Dopa (F-Dopa) has been used successfully to evaluate striatal dopaminergic function in humans. The kinetic analysis of F-Dopa studies, however, is confounded by the presence of [^{18}F]6-fluoro-3-O-methyl-L-Dopa (OMFD), the major metabolite of F-Dopa formed in the periphery that crosses the blood-brain barrier. We present results of compartmental analysis in subjects in whom we independently measured the kinetics of OMFD in the blood and striatum, and used this knowledge to solve for the kinetics of F-Dopa. **Methods:** The kinetics of F-Dopa in striatum were measured with PET from 0 to 150 min after an intravenous bolus injection of tracer in four normal subjects and two patients suffering from Parkinson's disease. On a separate occasion, the kinetics of OMFD were determined in the plasma and striatum of the same individuals. The measured OMFD kinetics of each individual allowed us to reduce the number of compartments and rate constants which have to be solved for any compartmental analysis of the kinetics of F-Dopa. **Results:** A two-compartmental, three rate-constant model was sufficient to describe the time course of F-Dopa and its metabolites in the striatum. The rate constant (k_{21}) representing the decarboxylation rate of F-Dopa was 0.0124 min^{-1} in the normal subjects, and 0.0043 min^{-1} in the parkinsonian patients. **Conclusion:** The data do not support the need to include a fourth rate constant representing the egress of F-Dopamine and its metabolites. The forward transport rates for F-Dopa and OMFD from plasma to striatum are very similar in humans.

Key Words: fluorine-18-F-Dopa; compartmental analysis; PET; dopamine metabolism; fluorine-18-OMFD

J Nucl Med 1996; 37:432–437

Dopamine is a neurotransmitter in the central nervous system found predominantly in the nigrostriatal neurons. Disturbances in dopamine metabolism are a key feature in neuro-degenera-

Received Jan. 4, 1995; revision accepted Jul. 5, 1995

For correspondence or reprints contact: Claude Nahmias, PhD, Department of Nuclear Medicine, McMaster University Medical Centre, 1200 Main St. West, Hamilton, Ontario, Canada, L8N 3Z5.

tive disorders such as Parkinson's disease (*1*). Dopamine is formed within neurons by the action of L-aromatic amino-acid decarboxylase (AADC) on its immediate precursor 3,4 dihydroxy-phenylalanine (L-Dopa) (*2*). Dopamine is stored in intraneuronal vesicles from which it is released when the nerve cell fires. The major metabolites of dopamine, through the action of monoamine oxidase (MAO) and catechol-O-methyl transferase (COMT), respectively are dihydroxy-phenyl acetic acid (DOPAC) and homovanillic acid (HVA); DOPAC itself also acts as a substrate for COMT, producing HVA.

Although dopamine in the circulation does not cross the blood-brain barrier (BBB), its immediate precursor, L-Dopa, is carried into the brain by the large neutral amino acid (LNAA) transport system. L-Dopa has been used successfully to relieve the symptoms of Parkinson's disease (*3*) and is also a substrate for COMT forming O-methyl-dopa (OMD). OMD, formed in peripheral organs and the circulation, is able to cross the BBB by the LNAA transport system (*4*).

An analog of L-Dopa labeled with the positron emitter ^{18}F, [^{18}F]6-fluoro-L-Dopa (F-Dopa), has been used successfully to trace the dopaminergic pathway and to evaluate striatal dopaminergic function (*5–7*). Like L-Dopa, F-Dopa crosses the BBB, is a substrate for AADC, is stored in neuronal vesicles as F-Dopamine and is catabolized to F-DOPAC and F-HVA (*8*). A number of researchers have attempted to derive values for the activity of AADC during life, but any definitive method of quantitative analysis is always confounded by the presence of other labeled species, formed in the periphery, and able to cross the BBB. F-Dopa is also a substrate for COMT forming [^{18}F]6-fluoro-3-O-methyl-L-Dopa (OMFD) which contributes to the radioactivity measured by the tomograph (*9*).

Compartmental models, which attempt to solve simultaneously for the kinetics of F-Dopa and OMFD, have been proposed by Huang et al. (*10*) and Kuwabara et al. (*11*). Both groups use a single, reversible compartment to model the kinetics of OMFD in the brain. Huang et al. (*10*) could not uniquely determine the forward transport rate of OMFD from blood to brain from a single striatal curve. They fixed this rate constant to be 1.7 times greater than that of F-Dopa. Kuwabara et al. (*11*) fixed the forward transport rate of OMFD to be 2.3 times greater than that of F-Dopa; this proportion is based on data that they obtained from rats (*12*). Recently, we reported the distribution and kinetics of OMFD measured in the human brain (*13*). The purpose of the present study was to examine the F-Dopa model in normal and parkinsonian individuals in whom we had also measured the time course of OMFD in blood and brain. These studies should provide definitive values for the activity of AADC as measured by the F-Dopa method.

METHODS

Tracer Preparation

F-Dopa and OMFD were synthesized in accordance to procedures previously described (*13*).

Scanning Procedure

Four normal male volunteers (aged 46, 20, 21 and 28 yr) and two male patients suffering from Parkinson's disease (aged 53 and 60 yr) were studied by PET after informed consent had been obtained. The controls had no history of recent medical illness, neurological disorders or substance abuse. The two patients were suffering from bilateral idiopathic Parkinson's disease lasting 3–5 yr duration. Both were on levodopa treatment, which was discontinued the evening before each examination. Each subject was studied twice during 1 wk: once after injection of between 5 and 10 mCi OMFD (specific activity: 2 Ci/m*M*) and once after injection of between 5 and 10 mCi of F-Dopa (specific activity: 2 Ci/m*M*). The studies were repeated in Subject 1 after a 6-mo interval. All subjects were studied after an overnight fast. On no occasion were the subjects pretreated with carbidopa.

Each subject was positioned in the scanner with his head immobilized by a headholder that allowed the brain to be covered by the axial field of view of the tomograph from the vertex to the cerebellum. Subjects were asked not to move during the study and were not spoken to for the duration of the examination. Low ambient lights and background noise defined the environment. Subjects' heads were positioned with respect to the orbito-meatal line, and the positioning was reproducible within a few millimeters on the two separate occasions.

Images were obtained with a tomograph that allowed simultaneous examination of 31 overlapping slices. The axial field of view was 10.8 cm and the spatial resolution was 6 mm (FWHM) in the three spatial dimensions. Images were reconstructed using a Hann filter with a cut-off frequency of 0.5. A 30-min transmission scan using a ^{68}Ge ring source was obtained before each study to correct for attenuation.

After a bolus injection of either F-Dopa or OMFD, subjects were scanned for 12 frames at 10 sec per frame, 6 frames at 30 sec per frame and 29 frames at 300 sec per frame for a total of 2.5 hr. In one subject, both studies were extended to 4 hr. Arterialized venous blood samples (5–10 ml) were taken throughout each study according to the following protocol: every 10 sec for the first 2 min; at 3, 4, 5, 7.5, 10, 12.5 and 15 min; at 20, 25, 30, 40, 50 and 60 min; at 75, 90, 105 and 120 min; and every 30 min thereafter. These blood samples were kept in ice before being centrifuged in a refrigerated centrifuge. Radioactivity in the plasma was counted in a well-counter, which had been calibrated to the tomograph. All samples were decay-corrected to the time of injection. These counts were corrected for injected dose and expressed as a percentage of injected counts per minute. The samples at 5, 10, 20, 60, 90 and 150 min were also assayed for tracer and other labeled metabolites. The concentration of amino acids in the plasma was measured before the start of each experiment and were within the normal range.

Regions of interest (ROIs) were identified on the F-Dopa studies with reference to a standard neuroanatomical atlas (*14*) and defined interactively around the left striatum and the right striatum at the most appropriate level. These ROIs were then transferred to the OMFD studies. The area of each region was on average 5.5 cm^2. The time course of radioactivity was calculated for each region expressed in counts per second per pixel. These counts were also corrected for dose injected and expressed in the same units as the plasma counts (fraction of cpm injected per ml) using the calibration factor between the well-counter and the tomograph. This was done so that tissue and blood data could be expressed in the same units and comparisons of the time course of radioactivity made between subjects (as in Figs. 3 and 4).

Metabolite Analysis

Fluorine-18-labeled metabolites of F-Dopa and OMFD in plasma were analyzed according to the method of McLellan et al. (*15*). This method measures the fraction of radioactivity in plasma associated with F-Dopa, OMFD or other labeled metabolites. Before and after each run, authentic F-Dopa and OMFD were mixed with plasma and run through the separation system. Recovery of these standards was better than 96%.

Data Analysis

OMFD Kinetics. The model used to describe the kinetics of OMFD in the striatum of each subject comprised a single, reversible compartment (Fig. 1) (*13*). The impulse response of this model was convolved with the plasma time-activity curve and compared

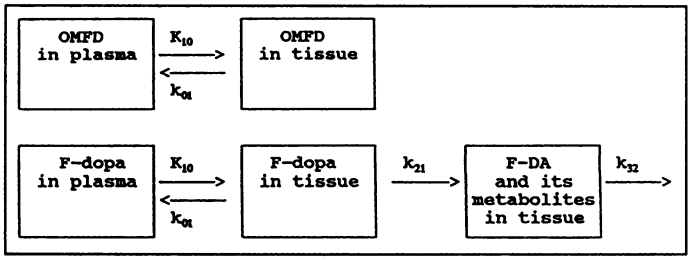

FIGURE 1. Compartmental model for describing the kinetics of OMFD and those of F-Dopa.

to the time course of radioactivity in each striatal region in each individual. Weighted least squares optimization of the rate constants was performed using an implementation of the Nelder-Meade simplex algorithm (*16,17*). This analysis determines the forward and backward transport kinetics for OMFD in each of the individual subjects.

F-Dopa Kinetics. The model used to describe the kinetics of F-Dopa in the striatum of each subject requires that the time course of radioactivity in the plasma due to F-Dopa alone be determined. The total radioactivity in plasma after F-Dopa is injected due to changing proportions of F-Dopa, OMFD and other metabolites of F-Dopa. The time course of F-Dopa in the plasma was determined using the approach of Chan et al. (*18*). The ratio of total metabolites of F-Dopa-to-F-Dopa alone was measured at six time points and the straight line relating these ratios to time (Fig. 2A) was used to calculate the amount of radioactivity at any time point that was due to F-Dopa alone. The time course of OMFD in the plasma was based on a model similar to that of Huang et al. (*19*), and used the measured proportion of OMFD relative to total radioactivity in the plasma at six different time points (Fig. 2B).

The time course of activity in the striatum due to OMFD alone was calculated by convolving the time course of OMFD in blood (Fig. 2C) with the impulse response of the OMFD model using the rate constants that had been measured independently in each subject. This contribution was then subtracted point-by-point from the total observed radioactivity to arrive at the time course of radioactivity in the striatum due to F-Dopa, F-Dopamine and the products of F-Dopamine metabolism (Fig. 4).

Using the time course of radioactivity due to F-Dopa alone in the plasma as an input function, and the time course of radioactivity due to F-Dopa, F-Dopamine and the products of F-Dopamine metabolism in the striatum as an output function, a compartmental analysis procedure was implemented. Progressively more complex models (Fig. 1) were solved and evaluated by an F-test (*20*). Weighted least squares optimization of the rate constants was performed using an implementation of the Nelder-Meade simplex algorithm (*16,17*).

Because it has been suggested that a rate constant representing the washout of products of metabolism from the field of view, k_{32} (*10*) or k_9^D (*11*), is needed, we explicitly included this parameter (k_{32}, Fig. 1) in a second stage of our analysis.

RESULTS

Figure 3 shows the striatal time-activity curves obtained in a normal subject (Fig. 3A) and a parkinsonian patient (Fig. 3B) after the injection of OMFD. The measured OMFD striatal curves were fitted well by a one-compartment, two-rate constant model. In the normal subjects, the forward transport rate constant for OMFD from plasma to striatal tissue was 0.0441 ml min^{-1} g^{-1}, the reverse transport rate constant was 0.0425 min^{-1}. In the parkinsonian patients, these rates were 0.0439 ml min^{-1} g^{-1} and 0.0422 min^{-1}, respectively (Table 1).

We observed the same significant linear relation between the ratio of total metabolites of F-Dopa-to-F-Dopa alone (Fig. 2A)

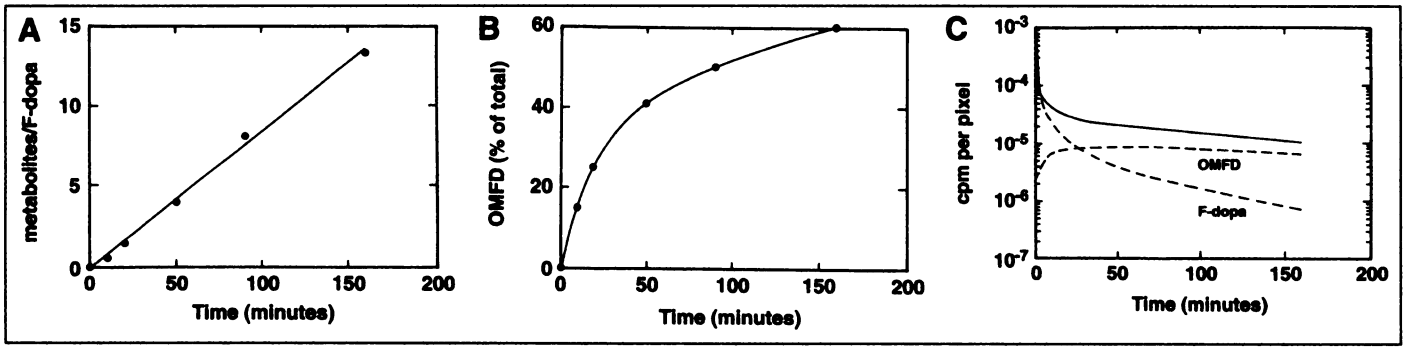

FIGURE 2. (A) Plot of the radioactivity ratio [total metabolites to F-Dopa] at different times after an injection of F-Dopa in a normal subject. Closed circles are data from the chemical separation; the solid line represents the results from the linear regression analysis. (B) Plot of OMFD (% of total plasma radioactivity) at different times after an injection of F-Dopa in a normal subject. Closed circles are data from the chemical separation; the solid line is the result of the fitting. (C) Plot of the time course of total ^{18}F radioactivity in plasma after an injection of F-Dopa in a normal subject (solid line). The curve for F-Dopa was calculated from the results of the analysis shown in (A). The curve for OMFD was calculated from the results of the analysis shown in (B).

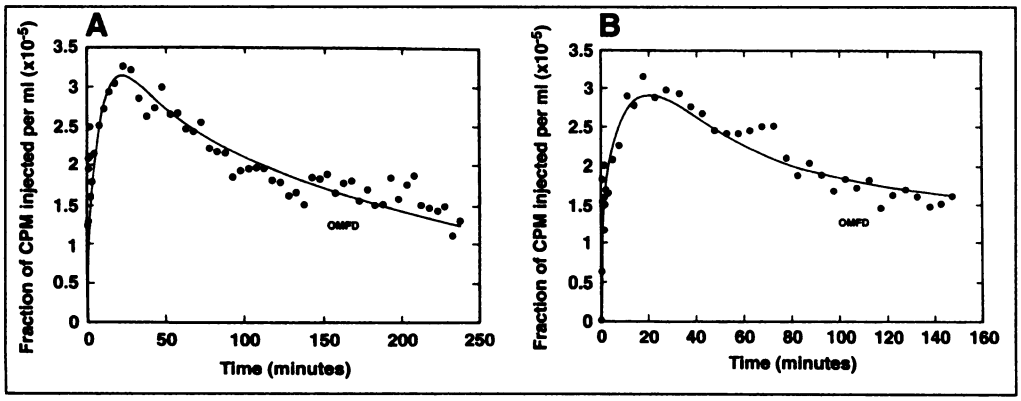

FIGURE 3. Time course of radioactivity in the striatum of a normal subject (A) and a parkinsonian patient (B) after an OMFD injection. Solid line represents the results from the compartmental analysis.

TABLE 1
Transport Kinetics of OMFD*

	Right striatum		Left striatum	
	K_{10} [ml min^{-1} g^{-1}]	k_{01} [min^{-1}]	K_{10} [ml min^{-1} g^{-1}]	k_{01} [min^{-1}]
Subject 1a	0.0512 (1.08)	0.0484 (1.12)	0.0498 (1.15)	0.0456 (1.21)
Subject 1b	0.0399 (1.13)	0.0374 (1.33)	0.0403 (1.65)	0.0353 (1.73)
Subject 2	0.0355 (1.08)	0.0435 (1.17)	0.0365 (1.01)	0.0410 (1.10)
Subject 3	0.0342 (1.06)	0.0293 (1.33)	0.0333 (1.09)	0.0304 (1.32)
Subject 4	0.0563 (1.26)	0.0577 (1.33)	0.0639 (1.16)	0.0573 (1.23)
Mean	0.0434 (1.12)	0.0432 (1.26)	0.0448 (1.21)	0.0419 (1.32)
Patient 1	0.0415 (1.45)	0.0413 (1.60)	0.0433 (1.46)	0.0459 (1.59)
Patient 2	0.0465 (1.26)	0.0429 (1.38)	0.0444 (1.29)	0.0390 (1.44)
Mean	0.0440 (1.35)	0.0421 (1.49)	0.0438 (1.37)	0.0424 (1.51)

*Standard deviation (%) of the rate constants estimated from the system covariance matrix

as Chan et al. (*18,21*). Our calculated regression coefficient ranged from 0.951 to 0.997; the slope ranged from 0.049 min^{-1} to 0.118 min^{-1}.

Figure 4 shows the striatal time-activity curves obtained in a normal subject (Fig. 4A) and a parkinsonian patient (Fig. 4B) after the injection of F-Dopa. The time course of striatal OMFD and that of F-Dopa, F-Dopamine and its metabolites are also shown in Figure 4. The curve representing the time course of F-Dopa and its metabolites was fitted well by a two-compartment, three-rate constant model. In the normal subjects, K_{10} was 0.0403 ml min^{-1} g^{-1}; k_{01} was 0.0342 min^{-1}; and k_{21} was 0.0124 min^{-1} (Table 2). The ratio of the forward transport rate constant for OMFD to that for F-Dopa was 1.12 (Table 2). The inclusion of a fourth rate constant in the analysis of the five studies in the control individuals did not significantly improve the fit (i.e., F value with (1,40) degrees of freedom was in all studies smaller than the threshold value of 4.08 for $p < 0.05$). When k_{32} is included in the analysis, its values were small and poorly determined as shown by their relatively large standard deviation (Table 3). The two 4-hr studies confirmed these conclusions: there was no significant improvement to the fits, as assessed by the F test, when k_{32} was included explicitly in the analysis (Table 4).

In the parkinsonian patients, a two-compartment, three-rate constant model fitted well the time course of F-Dopa and its metabolites in the striatum (Table 5). The ratio of the forward transport constant for OMFD to that for F-Dopa was 0.91. The inclusion of a fourth rate constant in the analysis did not significantly improve the fit (F value with (1,40) degrees of freedom was in the four cases analyzed smaller than the threshold value of 4.08 for $p < 0.05$).

DISCUSSION

A compartmental model which explicitly accounts for the contribution of OMFD was first proposed by Huang et al. (*22*) to study dopa decarboxylase activity in humans. The analysis was further refined by this group when Huang et al. (*10*) measured the kinetics of F-Dopa in striatum and cerebellum. They defined the time course of the arterial plasma concentrations of the tracer and its metabolites by biochemical assay. A two-compartment, three-rate constant model was used to describe the time course of radioactivity in the plasma. This approach was used to separate the contributions of F-Dopa and OMFD from the total plasma radioactivity. These contributions were then used as feeds to separate compartmental models which describe the kinetics of F-Dopa and OMFD in the striatum and cerebellum. This approach resulted in a two-compartment, six-rate constant model for the striatum. In the solution of the striatal compartmental model, one rate constant could not be uniquely determined and therefore the ratio of two rate constants had to be constrained (*10*).

Another approach was proposed by Gjedde et al. (*23*) and further studied by Kuwabara et al. (*11*). A two-compartment, two-parameter model was first analyzed by a graphical technique to determine the coefficient of methylation in the plasma and the loss of OMFD from the plasma. These values were used to construct the time course of F-Dopa and OMFD in plasma. A two-compartment, five-parameter model of an extrastriatal region of the brain was then solved by regression. The number of parameters was reduced to three by assuming: the ratio of the BBB clearance of F-Dopa to that of OMFD is constant for all subjects and equal to a value previously determined in the rat (*12*); this same ratio also applies to transport from the brain to the blood. A three-compartment, seven-parameter model for the striatum was similarly reduced to three parameters by making the above assumptions, plus the additional assumptions: the F-Dopa partition volume is equal in the two regions of the brain; and there is negligible methylation of F-Dopa in brain tissue. Dopa decarboxylase activity was measured by this method in 10 regions of the brain in six healthy volunteers (*23*).

We chose to independently measure the transport kinetics of OMFD across the BBB in a number of individuals, and to use these experimentally measured values to determine the kinetics of F-Dopa in the same individuals.

The rates of forward transport of OMFD and F-Dopa from plasma to striatal tissue are very similar in normal subjects and in subjects suffering from Parkinson's disease. The ratio of these forward rates is therefore close to unity. This is not surprising because both molecules are transported into the brain by the large neutral amino acid transport mechanism. Our experimental results do not support the constraint introduced by Huang et al. (*10*) who acknowledge that their model is

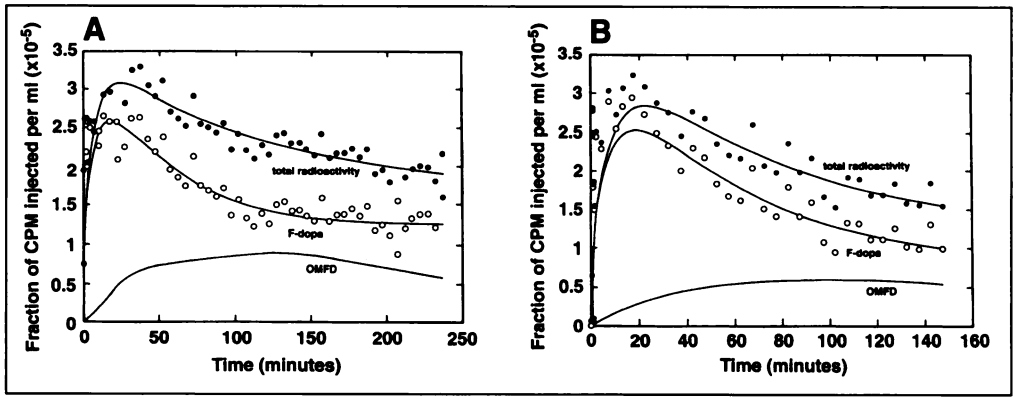

FIGURE 4. Time course of radioactivity in the striatum of a normal subject (A) and a parkinsonian patient (B) after an F-Dopa injection. Time course for OMFD was obtained by convolving the observed time course of OMFD in plasma (Fig. 2C) with the model parameters measured independently (Fig. 3).

TABLE 2
Transport Kinetics of F-Dopa in Striatum in Normal Subjects

Subject no.	K_{10} [ml min^{-1} g^{-1}]	k_{01} [min^{-1}]	k_{21} [min^{-1}]	K_{10}(OMFD) / K_{10}(F-Dopa)
1a	0.0388 (1.66)	0.0218 (2.45)	0.0067 (5.69)	0.98
1b	0.0323 (1.27)	0.0194 (1.97)	0.0067 (4.72)	1.25
2	0.0378 (1.14)	0.0566 (1.51)	0.0166 (2.10)	0.90
3	0.0227 (1.43)	0.0211 (2.63)	0.0122 (4.59)	1.59
4	0.0698 (1.07)	0.0522 (1.58)	0.0196 (2.15)	0.87
Mean	0.0403 (1.31)	0.0342 (2.03)	0.0124 (3.85)	1.12

TABLE 3
Transport Kinetics of F-Dopa in Striatum in Normal Subjects*

Subject no.	K_{10} [ml min^{-1} g^{-1}]	k_{01} [min^{-1}]	k_{21} [min^{-1}]	k_{32} [min^{-1}]
1a	0.0371 (1.71)	0.0224 (3.12)	0.0155 (6.54)	0.0047 (8.67)
1b	0.0357 (1.16)	0.0290 (1.99)	0.0179 (3.43)	0.0037 (6.45)
2	0.0400 (1.07)	0.0684 (1.49)	0.0231 (1.99)	0.0019 (10.2)
3	0.0213 (1.50)	0.0206 (3.36)	0.0200 (5.36)	0.0018 (17.4)
4	0.0682 (1.10)	0.0494 (1.59)	0.0189 (2.23)	0.0000 (700)
Mean	0.0405 (1.31)	0.0380 (2.31)	0.0191 (3.91)	0.0024 (148)

*Results of the 2-hr experiments with k_{32} included explicitly in the analysis.

over-determined. Our experimental results in humans also demonstrate that the ratio of the forward rate constants of OMFD and F-Dopa is quite different from that measured in the rat, thereby invalidating one of the assumptions made by Kuwabara et al. (*11*) in their analysis.

The data in normal subjects and in parkinsonian patients do not support the need to include a rate constant to account for the disappearance of the acid metabolites of F-Dopa, as postulated by Huang et al. (*10*) and Kuwabara et al. (*11*). Extending the period of observation to 4 hr, and thereby increasing the likelihood of observing this effect, clearly indicates that there is no justification for the inclusion of additional rate constants. It is interesting to note the agreement between our value for k_{21} (0.0124 min^{-1}) and that found by Huang et al. (*10*) when they set k_{32} explicitly to zero (0.0124 min^{-1}).

CONCLUSION

The forward transport rates for F-Dopa and OMFD from plasma to striatal tissue are very similar in humans. A simple two-compartment, three-rate constant model is adequate to describe the time course of F-Dopa, and its metabolites, in the striatum. These observations will considerably simplify any compartmental analysis for F-Dopa kinetics.

TABLE 4
Transport Kinetics of F-Dopa in Striatum in Normal Subjects*

Subject no.	K_{10} [ml min^{-1} g^{-1}]	k_{01} [min^{-1}]	k_{21} [min^{-1}]	k_{32} [min^{-1}]
1a	0.0364 (1.49)	0.0201 (2.16)	0.0068 (3.63)	0
	0.0372 (1.52)	0.0217 (2.22)	0.0081 (3.59)	0.0006 (34.5)
				[F = 1.03,(1,51), ns]
1b	0.0320 (1.19)	0.0191 (1.78)	0.0067 (2.99)	0
	0.0336 (1.19)	0.0229 (1.84)	0.0106 (2.89)	0.0015 (9.73)
				[F = 0.33,(1,51), ns]

*Results of the 4-hr experiments with k_{32} included explicitly in the analysis.

TABLE 5
Transport Kinetics of F-Dopa in Striatum in Parkinsonian Patients*

Patient no.	K_{10} [ml min^{-1} g^{-1}]	k_{01} [min^{-1}]	k_{21} [min^{-1}]	K_{10}(OMFD) / K_{10}(F-Dopa)
1				
Right striatum	0.0440 (2.13)	0.0246 (2.70)	0.0036 (9.62)	1.06
Left striatum	0.0443 (1.78)	0.0234 (2.44)	0.0047 (7.37)	1.00
2				
Right striatum	0.0594 (1.80)	0.0389 (2.18)	0.0056 (5.32)	0.70
Left striatum	0.0500 (3.31)	0.0256 (4.15)	0.0035 (15.8)	0.87
Mean	0.0494 (2.25)	0.0281 (2.86)	0.0043 (9.52)	0.91

*Standard deviation (%) of the rate constants estimated from the system covariance matrix.

ACKNOWLEDGMENTS

The authors thank Anita Scheffel for her untiring technical support, Margo Thompson for her help in the data collection, Dilip Murthy for the analysis of the plasma metabolites and Gunter Firnau and Raman Chirakal for the chemical syntheses. L.M. Wahl is the recipient of a Natural Sciences and Engineering Research Council Centennial (1967) Science Scholarship.

REFERENCES

1. Agid Y. Parkinson's disease: pathophysiology. *Lancet* 1991;337:1321–1324.
2. Lovenberg W, Weissbach H, Udenfriend S. Aromatic L-amino acid decarboxylase. *J Biol Chem* 1962;237:89–93.
3. Cotzias GC, Van Woert MH, Schiffer LM. Aromatic amino acid and modification of Parkinsonism. *N Engl J Med* 1967;276:374–379.
4. Oldendorf WH, Szabo J. Amino acid assignment to one of three blood-brain barrier amino acid carriers. *Am J Physiol* 1976;230:94–98.
5. Leenders KL, Salmon EP, Tyrrell P et al. The nigrostriatal dopaminergic system assessed in vivo by positron emission tomography in healthy volunteer subjects and patients with Parkinson's disease. *Arch Neurol* 1990;47:1290–1298.
6. Eidelberg D. Positron emission tomography studies in parkinsonism. *Neurologic Clinics* 1992;10:421–433.
7. Sawle GV. The detection of preclinical Parkinson's disease: what is the role of positron emission tomography? *Movement Disorders* 1993;8:271–277.
8. Melega WP, Grafton ST, Huang SC, Satyamurthy N, Phelps ME, Barrio JR. L-6-[^{18}F]fluoro-DOPA metabolism in monkeys and humans: biochemical parameters for the formulation of tracer kinetic models with positron emission tomography. *J Cereb Blood Flow Metab* 1991;11:890–897.
9. Melega WP, Luxen A, Perlmutter MM, Nissenson CHK, Phelps ME, Barrio JR. Comparative in vivo metabolism of 6-[^{18}F]fluoro-L-Dopa and [^{3}H]L-Dopa in rats. *Biochem Pharmacol* 1990;39:1853–1860.
10. Huang SC, Yu DC, Barrio JR, et al. Kinetics and modeling of L-6-[F-18]fluoro-DOPA in human positron emission tomographic studies. *J Cereb Blood Flow Metab* 1991;11:898–913.
11. Kuwabara H, Cumming P, Reith J, et al. Human striatal L-DOPA decarboxylase activity estimated in vivo using 6-[F-18]fluoro-DOPA and positron emission tomography: error analysis and application to normal subjects. *J Cereb Blood Flow Metab* 1993;13:43–56.
12. Reith J, Dyve S, Kuwabara H, Guttman M, Diksic M, Gjedde A. Blood-brain transfer and metabolism of 6-[^{18}F]Fluoro-L-Dopa in rat. *J Cereb Blood Flow Metab* 1990;10:707–719.
13. Wahl L, Chirakal R, Firnau G, Garnett ES, Nahmias C. The distribution and kinetics of [^{18}F]6-fluoro-3-O-methyl-L-Dopa in the human brain. *J Cereb Blood Flow Metab* 1994;14:664–670.
14. Talairach J, Tournoux P. *Co-planar stereotaxic atlas of the human brain*. New York: Thieme; 1988.
15. McLellan CA, Doudet DJ, Brucke T, Aigner TG, Cohen RM. New rapid analysis method demonstrates differences in 6-[F-18]fluoro-L-Dopa plasma input curves with and without carbidopa and in hemi-MPTP lesioned monkeys. *Appl Radiat Isot* 1991;42:847–854.
16. The MathWorks, Inc. *PRO-MATLAB user's guide*. Natick, MA: The MathWorks, Inc.; 1990.
17. Press WH, Flannery BP, Teukolsky SA, Vetterling WT. *Numerical recipes: the art of scientific computing*. Cambridge: Cambridge University Press; 1986:289–293.
18. Chan GLY, Morrison KS, Holden JE, Ruth TJ. Plasma L-[F-18]6-fluorodopa input function: a simplified method. *J Cereb Blood Flow Metab* 1992;12:881–884.

19. Huang SC, Barrio JR, Yu DC, et al. Modelling approach for separating blood time-activity curves in positron emission tomographic studies. *Phys Med Biol* 1991;36:749–761.
20. Landaw EM, DiStephano JJ. Multiexponential, multicompartmental, and noncompartmental modeling. II. Data analysis and statistical considerations. *Am J Physiol* 1984;246:R655–R677.
21. Chan GLY, Hewitt KA, Pate BD, Schofield P, Adam MJ, Ruth TJ. Routine determination of [^{18}F]-L-6-fluorodopa and its metabolites in blood plasma is essential for accurate positron emission tomography studies. *Life Sciences* 1991; 50:309–318.
22. Huang SC, Barrio JR, Hoffman JM, et al. A compartmental model for 6-[F-18]fluoro-L-DOPA kinetics in cerebral tissues [Abstract]. *J Nucl Med* 1989;30:735.
23. Gjedde A, Reith J, Dyve S, et al. Dopa decarboxylase activity of the living human brain. *Proc Natl Acad Sci* 1991;88:2721–2725.

Evaluation of Lung Ventilation and Alveolar Permeability in Cirrhosis

Chia-Hung Kao, Chih-Kua Huang, Shih-Chuan Tsai, Shyh-Jen Wang and Gran-Hum Chen
Department of Nuclear Medicine and Division of Gastroenterology, Taichung Veterans General Hospital, Taiwan, Republic of China

This study sought to evaluate lung ventilation and alveolar permeability (AP) in patients with cirrhosis of the liver. **Methods:** Pulmonary function in 29 patients with cirrhosis was measured by ^{99m}Tc-DTPA aerosol inhalation lung scintigraphy, using commercial lung radioaerosol delivery units. Equilibrium lung ventilation images were visually interpreted according to the presence or absence of inhomogeneous distribution, inverted base-to-apex gradient and segmental defects. Degree of AP damage to the upper, middle, lower and total right lung was expressed as the slopes of the time-activity curves from dynamic lung images. The patients were classified into three groups, according to cirrhotic severity, using the modified Child's classification (A = good; B = fair; C = poor). Twelve healthy nonsmokers (2 women, 10 men; 42–75 yr old) formed the control group, and all had normal chest radiographic and pulmonary function test results. **Results:** None of the 29 patients had significantly abnormal lung ventilation findings, but 13 had reduced lung ventilation in the basilar lung zone. The incidence of lung ventilation abnormalities was 20% (3 of 15), 50% (3 of 6) and 88% (7 of 8) in patients with nil, slight-to-moderate and moderate-to-severe ascites, respectively ($p < 0.05$ for nil versus moderate-to-severe ascites). The AP studies showed higher time-activity curve slopes for patients with cirrhosis than for normal control subjects. The slopes for the right total lung showed no significant differences among the three groups; however, those for right upper and right lower lung showed significant differences between some subgroups. In addition, albumin and bilirubin levels showed no significant correlation with slope values in cirrhotic patients. **Conclusion:** Although lung ventilation is normal in most patients with cirrhosis of the liver (16 [55%] of 29 in the present study), the disease can predispose patients to AP damage; however, the degree of damage is not related to cirrhotic severity.

Key Words: cirrhosis; lung ventilation; alveolar permeability
J Nucl Med 1996; 37:437–441

Impairment of pulmonary function has long been associated with severe hepatic disease (*1,2*); however, the physiological mechanism of impairment has not been completely elucidated. In recent years there has been an increase in the use of ^{99m}Tc-DTPA radioaerosols for clinical investigations. Aerosols have replaced radioactive gases, such as ^{81m}Kr and ^{133}Xe, at some centers. Technetium-99m-DTPA radioaerosols, generated by a jet nebulizer, are inexpensive, readily available and have good scintigraphic quality. Technetium-99m-DTPA radioaerosols have been used to visualize lung ventilation (*3–5*) and to evaluate alveolar permeability (AP) (*6–10*) in various diseases. The present study sought to evaluate ^{99m}Tc-DTPA radioaerosol lung scintigraphic changes in lung ventilation and AP in patients with cirrhosis of the liver.

Received Jan. 11, 1995; revision accepted Jun. 17, 1995.
For correspondence or reprints contact: Chia-Hung Kao, MD, Department of Nuclear Medicine, Taichung Veterans General Hospital, 160 Taichung Harbor Road, Section 3, Taichung 40705, Taiwan, Republic of China.

MATERIALS AND METHODS

Patients

Twenty-nine patients (3 women, 26 men; aged 36–75 yr) with cirrhosis of the liver secondary to chronic hepatitis were included in the study. The patients were classified into three groups according to severity of liver cirrhosis, using the modified Child's classification, which takes into account encephalopathy, ascites, bilirubin and albumin levels, prothrombin index and prothrombin time: class A = good; class B = fair; class C = poor (*11*). The AP of patients with cirrhosis was compared with that of 12 normal control subjects (2 women, 10 men; 42–75 yr old). No control subject had a history of smoking, and all chest radiographic findings and pulmonary function test results were normal (Table 1).

Radioaerosol Inhalation Lung Scintigraphy

Technetium-99m was chelated to DTPA by introducing 50 mCi pertechnetate into a vial containing 20 mg DTPA and 2.2 mg tin chloride. Technetium-99m-DTPA was prepared no more than 1 hr before use, and ^{99m}Tc-DTPA radioaerosol was generated by a commercial lung aerosol delivery unit that contained 20 mCi ^{99m}Tc-DTPA in 2 ml saline. Radioaerosol droplet size was measured by an inertial impactor. The mass median aerodynamic diameter of the ^{99m}Tc-DTPA radioaerosol was smaller than 1 μm, with an oxygen air flow rate of 7 liters/min. All subjects were studied in the supine position, and they inhaled for 2 min from the aerosol delivery unit until the total radioactivity was more than 200,000 counts by normal tidal breathing. Data were collected for another 30 min by means of a large-field computerized gamma camera over the posterior view that included the entire chest. The data were acquired as a series of 30 consecutive frames of 1-min duration each in a 64 × 64 matrix with word mode.

Data Analysis

Lung Ventilation. After background correction, the first image in the series was selected as the equilibrium lung ventilation image. Two independent observers judged the lung ventilation images according to established criteria (*12,13*), which included the presence or absence of inhomogeneous distribution, inverted base-to-apex gradient, segmental defects and basilar hypoventilation.